Piezoelectric potential in vertically aligned nanowires for high output nanogenerators

2011 Nanotechnology 22 465401

(http://iopscience.iop.org/0957-4484/22/46/465401)

Nanotechnology **22** (2011) 465401 (6pp) doi:10.1088/0957-4484/22/46/465401

Piezoelectric potential in vertically aligned nanowires for high output nanogenerators

Giuseppe Romano[1,3,4], Giulia Mantini[1], Aldo Di Carlo[1], Arnaldo D'Amico[1,2], Christian Falconi[1,2] and Zhong Lin Wang[3]

[1] Department of Electronics Engineering, University of Rome 'Tor Vergata', I-00133 Rome, Italy
[2] CNR IDAC, via Fosso del Cavaliere, 100, I-00133 Rome, Italy
[3] School of Materials Science and Engineering, Georgia Institute of Technology, 771 Ferst Drive NW, Atlanta, GA 30332, USA
[4] Department of Materials Science and Engineering, Massachusetts Institute of Technology, 77 Massachusetts Avenue, Cambridge, MA 02139, USA

E-mail: romanog@mit.edu

Received 15 August 2011, in final form 12 September 2011
Published 24 October 2011
Online at stacks.iop.org/Nano/22/465401

Abstract
In this work we analyze the coupled piezoelectric and semiconductive behavior of vertically aligned ZnO nanowires under uniform compression. The screening effect on the piezoelectric field caused by the free carriers in vertically compressed zinc oxide nanowires (NWs) has been computed by means of both analytical considerations and finite element calculations. We predict that, for typical geometries and donor concentrations, the length of the NW does not significantly influence the maximum output piezopotential because the potential mainly drops across the tip, so that relatively short NWs can be sufficient for high-efficiency nanogenerators, which is an important result for wet-chemistry fabrication of low-cost, CMOS- or MEMS-compatible nanogenerators. Furthermore, simulations reveal that the dielectric surrounding the NW influences the output piezopotential, especially for low donor concentrations. Other parameters such as the applied force, the sectional area and the donor concentration have been varied in order to understand their effects on the output voltage of the nanogenerator.

(Some figures in this article are in colour only in the electronic version)

ZnO nanostructures and nanodevices have recently broadened the spectrum of potential applications of nanomaterials, in particular in the field of energy harvesting [1]. ZnO is a semiconductor material, which exhibits a large direct bandgap, large exciton binding energy and piezoelectric properties. A wide variety of ZnO nanostructures have been synthesized: nanobelts [2], nanowires [3], nanorings [4] and nanohelices [5]. Since the first demonstration of the feasibility of piezoelectric nanogenerators [6], arrays of ZnO nanowires have been employed in a variety of devices, such as a direct current generator driven by ultrasonic waves [7], piezoelectric nanogenerator on plastic substrates [8], single-wire nanogenerator [9] and muscle-driven *in vivo* nanogenerator [10].

More recently, it has been demonstrated that an array of vertically aligned ZnO NWs, under uniaxial compression, is able to power a nanodevice, in particular a PH sensor [11]. The magnitude of the output potential produced by the compressed NW is a result of a competition between the piezoelectric field generated by the force applied on the NW and the screening effect due to the free charge carriers. Indeed, depending on the synthesis conditions, as-grown ZnO NWs are typically n-type with a donor concentration ranging from 10^{16} to 10^{17} cm^{-3} [12–14].

While the exact interplay of such effects for laterally bent NWs has already been investigated [15, 16] an electromechanical analysis of vertically compressed semiconductive NWs is still lacking. In addition, geometry, doping concentration and applied force may have a great impact on the performance of the nanogenerator. An accurate model of vertically compressed NWs going beyond simple considerations is therefore necessary in order to properly design high output nanogenerators.

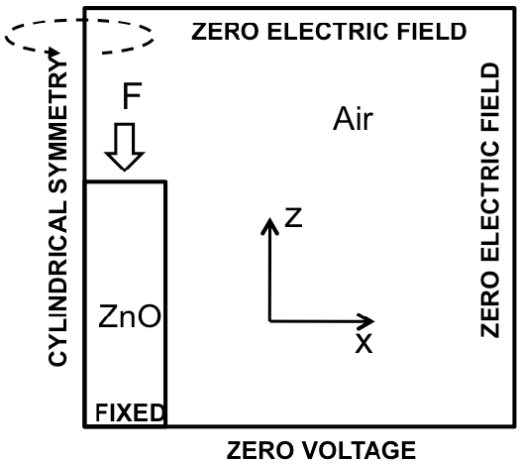

Figure 1. The simulation domain is composed by a ZnO NW grounded and fixed at its base and pushed by a uniaxial compressive force along the z axis, exerted at its tip. The cylindrical symmetry is used to simplify the model, so only half space has been simulated. The ZnO NW is surrounded by an external medium. The far-field boundary conditions are zero voltage at the base of the domain and zero electric field far away from the NW.

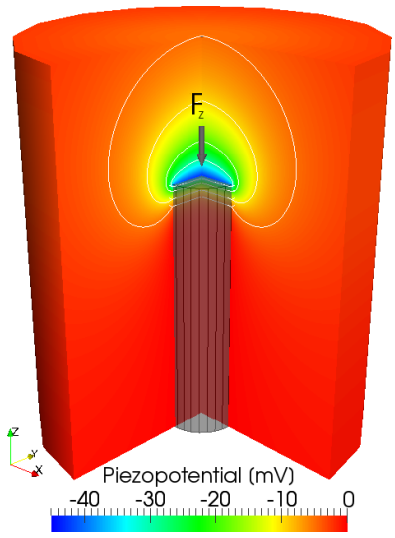

Figure 2. Piezoelectric potential distribution for a 1×10^{16} cm^{-3}-doped ZnO NW with $R = 150$ nm and $L = 4$ μm pushed by a uniaxial compressive force (along the z axis). The maximum piezoelectric potential is experienced at the top of the NW with a value of about -43 mV. The base of the NW is grounded and fixed. Equipotential lines are also shown in figure.

In this work we perform a theoretical and finite element analysis of a vertically compressed NW under equilibrium conditions and considering a finite electrical conductivity. The piezoelectric maps obtained by varying the above-mentioned parameters are presented and discussed. Details about the theoretical bases on the electromechanical modeling of piezoelectric nanowires will also be given.

1. Result and discussions

Investigating the experimental configuration presented in [11] for the vertically integrated nanogenerator, we assume that a ZnO NW epitaxially grown along the c axis on a single-crystal substrate is pushed by a uniaxial force exerted at its tip. According to [11], the NW is modeled as a cylinder oriented along the z axis, with a radius $R = 150$ nm and a length $L = 4$ μm. A pressure $P = 6.25$ MPa is uniformly applied on the top surface of the NW, parallel to its growth axis, corresponding to a punctual force of $F = -442$ nN where the sign is negative because the force is compressive. The base of the NW is fixed to the substrate. The vertical compression produces a uniform uniaxial strain along the NW. By assuming isotropic elastic constants, the components of the strain tensor are $\varepsilon_{zz} = \frac{F}{E\pi R^2}$, $\varepsilon_{xx} = \varepsilon_{yy} = -\frac{F\nu}{E\pi R^2}$ and $\varepsilon_{xy} = \varepsilon_{xz} = \varepsilon_{yz} = 0$, where $E = 129$ GPa and $\nu = 0.349$ are the Young's modulus and Poisson's ratio of ZnO, respectively. These values are consistent with previous literature [16, 17], where the isotropic model has been found to be an excellent approximation, with an error smaller than 3.27% with respect to the ZnO elastic constant [19]. Under uniaxial compressive strain, the wurtzite cell will be deformed so that a bound charge will be present at both ends of the NW, thus creating a dipole-like piezopotential along the c axis. Thanks to the piezoelectric effect, the strain produces a polarization field $P_i = e_{ilk}\varepsilon_{lk}$, where e_{ilk} are the piezoelectric coefficients, described by the tensor

$$e = \begin{pmatrix} 0 & 0 & 0 & 0 & e_{15} & 0 \\ 0 & 0 & 0 & e_{15} & 0 & 0 \\ e_{31} & e_{31} & e_{33} & 0 & 0 & 0 \end{pmatrix}.$$

$e_{31} = -0.51$ C m^{-2}, $e_{33} = 1.22$ C m^{-2} and $e_{15} = -0.45$ C m^{-2} are measured for ZnO films in [20]. The resulting piezoelectric field is oriented along the NW growth axes and its value is $P_z = e_{31}(\varepsilon_{xx} + \varepsilon_{yy}) + e_{33}\varepsilon_{zz}$.

Before we investigate the piezopotential profile of a semiconductive NW, we first analyze the piezoelectric potential of an intrinsic NW. The Poisson equation, in the absence of free carriers and including the piezoelectric field, is $\nabla \cdot (\kappa_0\kappa_r\mathbf{E} + \mathbf{P}) = 0$, where $\mathbf{E}$ is the electric field, κ_0 is the dielectric constant of vacuum and κ_r is the relative dielectric constant, which has the form

$$\kappa_r = \begin{pmatrix} \kappa_\perp & 0 & 0 \\ 0 & \kappa_\perp & 0 \\ 0 & 0 & \kappa_\parallel \end{pmatrix}$$

where the components $\kappa_\perp = 7.77$ and $\kappa_\parallel = 8.91$ are the values measured for bulk ZnO in [21]. The base of the NW is connected to ground and is at the reference potential. The lateral and the top surface are imposed to have zero surface charge, i.e. $(\kappa_0\kappa_r\mathbf{E} + \mathbf{P}) \cdot \mathbf{n} = 0$, where $\mathbf{n}$ is the vector normal to the surface. It is straightforward to show that, under this condition, the piezoelectric potential is constant along the sectional area and its trend along the z axis can be obtained by solving the 1D Poisson equation:

$$\frac{\partial}{\partial z}\left(\kappa_0\kappa_\parallel \frac{\partial \varphi(z)}{\partial z} - P_z\right) = 0. \quad (1)$$

Equation (1) gives a linear potential profile $\varphi(z) = (\kappa_0\kappa_\parallel)^{-1} P_z z$, where the conditions $E_z(L) = -(\kappa_0\kappa_\parallel)^{-1} P_z$

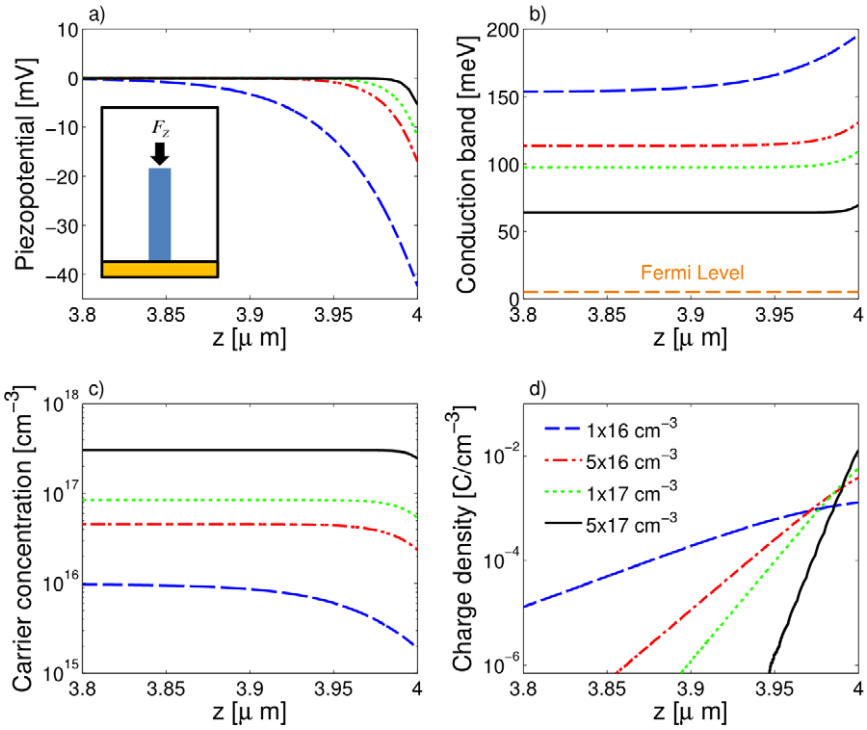

Figure 3. (a) Piezoelectric potential distribution of a semiconductive ZnO NW ($R = 150$ nm and $L = 4$ μm) pushed by a uniaxial compressive force of 442 nN (corresponding to a pressure $P = 6.25$ MPa) for different donor concentrations. The lineplot is taken along the z axis at $x = 0$ and $y = 0$ and refers to the last 300 nm of the upper part of the NW. The piezoelectric potential is almost completely screened for a donor concentration of about $N_D = 5 \times 10^{17}$ cm^{-3}. The conduction bands and electron density in the presence of free charge carriers are shown in (b) and (c), respectively. The conduction bands, which are refereed to the Fermi level (set to zero), are deflected in the region near the top of the NW, but increasing the donor concentration the conduction bands tends to reach the Fermi level, thus screening the piezoelectric potential. In (d) the total charge density, computed as $\rho = q(N_D^+ - n)$, is shown.

and $\varphi(0) = 0$ have been used. The maximum piezopotential magnitude is therefore $\varphi_{max} = |\varphi(L)|$, i.e.

$$\varphi_{max} = \left| F_z \left(\frac{e_{33} - 2\nu e_{31}}{E\kappa_0\kappa_\parallel} \right) \frac{L}{\pi R^2} \right| = |F_z| \gamma_V \frac{L}{\pi R^2} = 3.87 \text{ V} \tag{2}$$

where $\gamma_V = 0.1549$ V m^{-1} is a property of the material. Equation (2) should be compared with the expression of the maximum piezopotential (of the negative side) of a laterally deflected NW with the same geometry and magnitude of the applied force [17]:

$$\varphi_{max} = \left| F_y \left(\frac{e_{33} - 2\nu e_{31} - 2(1+\nu)e_{15}}{E\kappa_0(1+\kappa_\perp)} \right) \frac{1}{\pi R} \right|$$
$$= |F_y| \gamma_L \frac{1}{\pi R} = 0.26 \text{ V} \tag{3}$$

where $|F_y| = |F_z|$ and $\gamma_L = 0.2787$ V m^{-1}. These results are in agreement with those given in [22], where the dimension and position of the electrical contacts, as well as the direction of the input force, are systematically compared in the most important configurations for two-contact piezoelectric NWs. In particular, taking into account a force applied at the free tip of the NW, it has been shown that the presence of the conductive film at the base of the NW, which is also the region experiencing the highest strain, significantly reduces the output potential. By contrast, in the case of vertical compression or lateral stretching, where the strain is more uniformly distributed, the presence of continuous conductive films at the base or tip of the NW does not reduce the output potential. This observation, first proposed in [22], gives an explanation of the practical advantages of the configurations presented in [9] for lateral stretching, and in [11] for vertical compression. The two configurations reach the same maximum potential output for a shape factor $S = \frac{R}{L} = \frac{\gamma_V}{\gamma_L} \cong 0.5558$. For higher values of S which, however, would result in impractically small NWs, the laterally deflected NW would present a higher piezopotential.

Let us now analyze the effect of the free carriers on the piezoelectric potential. Due to the complexity of the charge carrier dynamics we have performed finite element (FE) calculations in order to get a realistic trend for the piezoelectric potential inside the NW.

FE simulations have been carried out by means of TiberCad, a multiscale simulator for electronic devices [23, 24]. Our simulations are restricted to the static analysis of the open circuit voltage (i.e. Thevenin voltage) of vertically compressed nanowires (e.g. similar to [15–22]). The simulation domain comprises the NW surrounded by air in order to properly set the boundary conditions at infinite distance from the NW (i.e. zero electric field). The presence of the substrate is modeled connecting to ground the entire bottom surface of the simulation domain, which is set to zero potential. Furthermore, taking advantage of the symmetry of the system, we restricted the simulations to the half-space $x > 0$ and then applied the

cylindrical symmetry (see figure 1). The Poisson equation now includes the free carriers and is

$$\frac{\partial}{\partial x_i}\left(\kappa_{ij}\frac{\partial \varphi}{\partial x_j}\right) = -e(N_{\mathrm{D}}^{+} - n) + \frac{\partial}{\partial x_i}P_i. \tag{4}$$

The ionized donor concentration N_{D}^{+} is a function of the temperature and is given by

$$N_{\mathrm{D}}^{+} = N_{\mathrm{D}}\frac{1}{1 + 2\exp(\frac{E_{\mathrm{F}} - E_{\mathrm{C}} - \Delta E_{\mathrm{D}}}{k_{\mathrm{B}}T})}. \tag{5}$$

In equation (5) $E_{\mathrm{C}} = 3.34$ eV is the conduction band edge, E_{F} is the Fermi level, which is set to zero, $\Delta E_{\mathrm{D}} = 0.035$ eV [21] is the level of the donor below the conduction band, k_{B} is Boltzmann's constant and $T = 300$ K is the temperature. The electrons concentration n is computed by considering parabolic electron bands:

$$n = N_{\mathrm{C}}F_{1/2}\left(\frac{e\varphi + E_{\mathrm{F}} - E_{\mathrm{C}}}{k_{\mathrm{B}}T}\right). \tag{6}$$

In equation (7) $F_{1/2}(x)$ is the Fermi–Dirac integral of order $\frac{1}{2}$ function and N_{C} is the effective density of states for electrons given by

$$N_{\mathrm{C}} = 2\left(\frac{2\pi m_{\mathrm{e}}k_{\mathrm{B}}T}{h^2}\right)^{\frac{3}{2}} \tag{7}$$

where $m_{\mathrm{e}} = 0.28m_0$ [25] is the electron effective mass and h is Planck's constant.

Figure 2 shows a 3D cut of the piezopotential profile for $N_{\mathrm{D}} = 1 \times 10^{16}$ cm^{-3} whereas figures 3(a) and (b) show the piezoelectric potential and the conduction band profile, respectively, at the top of the NW for different donor concentrations ranging from $N_{\mathrm{D}} = 1 \times 10^{16}$ cm^{-3}, where $\varphi_{\max} \cong 42$ mV, to $N_{\mathrm{D}} = 5 \times 10^{17}$ cm^{-3}, where $\varphi_{\max} \cong 5$ mV. As we can see from figure 3(a), the higher the donor concentration is, the lower the magnitude of the piezopotential is and, therefore, the more pronounced the piezoelectric field screening due to free carriers is. Indeed, at a donor concentration as high as $N_{\mathrm{D}} = 5 \times 10^{17}$ cm^{-3}, the negative side is almost completely screened. When a compressive force is applied to the NW, electrons close to the tip will deplete (figure 3(c)) so that a positive charge, given by ionized donors, will balance the negative charge along the top surface, created by the external force. The depletion region leads to a potential drop close to the tip of the NW, which can be interpreted as the piezopotential output. In figure 4, the piezopotential maps close to the tip for different donor concentrations are shown. With a donor concentration of $N_{\mathrm{D}} = 1 \times 10^{16}$ cm^{-3}, our model predicts a magnitude of the output potential which is consistent with experimental results [11]; differences can be attributed to different and non-homogeneous doping, different mechanical and piezoelectric parameters, NW misalignment and the unavoidable weak shear component of the applied force in real devices. As shown in figure 4, as the donor concentration increases the width of the depletion region decreases. The charge density, given by the sum of the ionized donors and electron concentrations (the hole concentrations can be neglected because the NW is n-doped) is $\rho = q(N_{\mathrm{D}}^{+} - n)$ and is plotted in figure 3(d). If we consider a full depletion approximation (i.e. there is an abrupt transition between a fully depleted region with uncompensated fixed charges and a neutral region) the width of the depletion region would be $\Delta z = \frac{|P_z|}{qN_{\mathrm{D}}^{+}}$. Even for a doping concentration as low as $N_{\mathrm{D}} = 1 \times 10^{16}$ cm^{-3} the depletion width is about $\Delta z = 45$ nm; clearly, for higher doping levels the depletion region is even smaller; as a result, in practical nanowires the depletion region is much smaller than the lengths. Moreover, under the full depletion approximation, there is no voltage drop outside the depletion region and, therefore, increasing the length of practical nanowires would result in no variation of the output piezopotential (see figure 5(a)). Our FE simulations demonstrate that, though, obviously, the transition between depletion and neutral regions is not ideally sharp, as shown in figure 3(d), our conclusion on the almost complete independence of the maximum piezopotential on the nanowire length is correct. This result can be extremely important for practical implementations; for instance, despite many important practical advantages (low cost, high yield, high area and low-temperature processing) wet-chemistry methods for growing NWs do not presently allow us to grow ZnO NWs longer than a few microns [26]; our simulations demonstrate that this limit can be relatively unimportant for the design of high-efficiency nanogenerators. We have extended our analysis

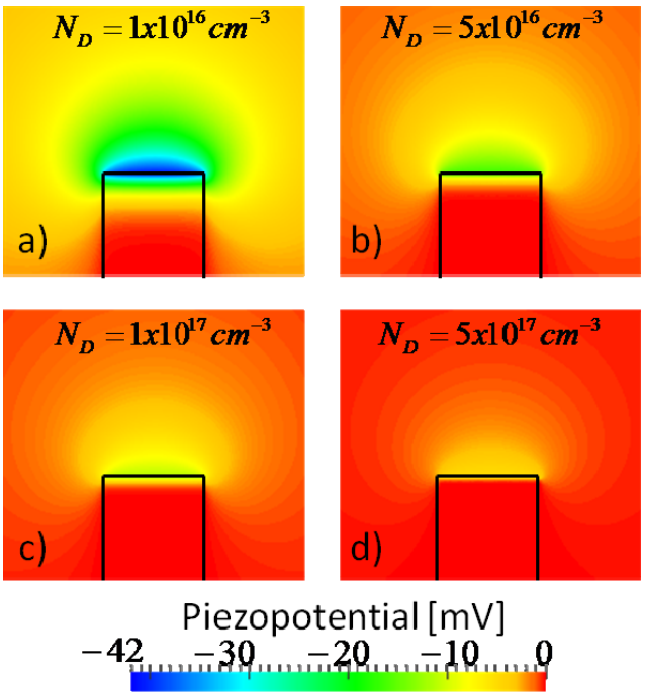

Figure 4. Piezoelectric potential distribution of a ZnO NW vertically compressed along the z axis by a force exerted at its tip. Only the region near the tip of the NW is shown here in order to better understand the role played by donors. Increasing the donor concentrations (from (a) to (d)) the piezoelectric potential will be almost completely screened by free charge carriers. For clarity, a proper colormap has been used (i.e. with very small relative extension of the red region, so that very small piezopotentials can be distinctly observed).

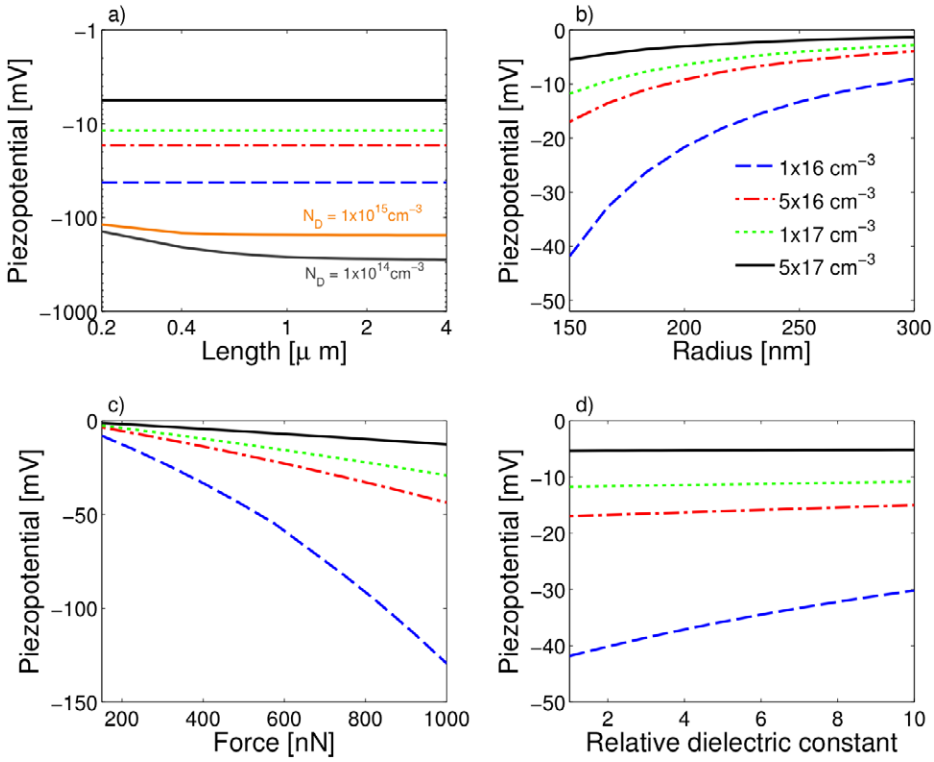

Figure 5. Piezoelectric potential of a ZnO NW pushed by a uniaxial compressive force of 442 nN for different donor concentrations. The value plotted is that one experienced at the top of the NW. (a) The length sweeps from $L = 200$ nm to 4 μm whereas $R = 150$ nm. For higher donor concentrations the output potential is length-independent because the width of the depletion region is small compared to the length of the NW. (b) The radius is varied from $R = 150$ to 300 nm whereas the length is $L = 4$ μm. An increase in the area will reduce the pressure applied at the top of the NW (we consider a constant applied force), thus decreasing the output piezopotential. On the other hand, if we increase the force (c) and keep constant the sectional area, the magnitude of the piezopotential will increase with a pretty linear trend, as it happens for the intrinsic NW. (d) The relative dielectric constant of the external medium is varied between 1 (air) and 10.

to hypothetical nanowires with doping concentrations as low as $N_D = 1 \times 10^{15}$ and 1×10^{14} cm^{-3} and lengths as low as $L = 200$ nm; for such hypothetical nanowires the width of the depletion region becomes comparable with the NW length and, therefore, the maximum piezopotential becomes length-dependent.

When increasing the radius of the NW and keeping constant all the other parameters, the pressure applied at the top of the NW will decrease, due to the increase of the cross-sectional area (see figure 5(b)). The piezopotential will almost cut its value in half, for an increase of the area by a factor of 3 (the diameter is doubled). Figure 5(c) shows the influence of the applied force on the piezoelectric potential. In the intrinsic case, there is a linear relation between the force and the output potential, in accordance with equation (2). The relationship does not maintain its perfect linearity when considering free charge carriers at different donor concentrations. Indeed, especially for lower donor concentrations the trend appears to be pretty parabolic.

Finally, we have investigated the influence of the dielectric properties of the material around the NW. In general, the bigger the relative dielectric constant is, the lower is the piezopotential output. However, the reduction of the output potential is more relevant for low donor concentrations and becomes negligible at sufficiently high donor concentrations. This result may also be crucial for the design of high-efficiency nanogenerators; for instance, in order to enhance the mechanical stability of nanogenerators, in [11] the authors wrap the NW with a spin-coated polymethyl-methacrylate (PMMA), whose relative dielectric constant is about 2.6. From figure 5(d), it becomes clear that even a relatively low donor concentration (e.g. $N_D = 1 \times 10^{16}$ cm^{-3}) is sufficient to make the reduction of the piezopotential induced by the dielectric constant of PMMA negligible; on the other hand, in close-to-intrinsic NWs, the dielectric constant of PMMA might significantly reduce the piezopotential.

In summary, in this work we have performed a theoretical and finite element analysis of a vertically compressed semiconductive ZnO NW. The boundary conditions take into account the presence of a conductive thin film at the bottom of the NW. We computed the output piezoelectric potential by varying the donor concentrations, the physical geometry, the applied force and the dielectric material surrounding the NW. Our results provide important guidelines for the design of high-efficiency piezoelectric nanogenerators. First, we found that for a donor concentration of $N_D = 1 \times 10^{16}$ cm^{-3} the magnitude of the maximum output potential is about $\varphi_{max} = 42$ mV, comparable with previous experimental results, and we determined the output potential for different donor concentrations. Furthermore, since most of the potential drop

occurs in the region close to the tip of the NW, the length of the NW does not significantly affect the maximum value of the piezopotential, so that even relatively short piezoelectric NWs can be used for high output nanogenerators; this suggests that an apparently relevant limit of the (low-cost, simple, high yield, low-temperature, CMOS- and MEMS-compatible) wet-chemistry method for growing ZnO NWs may actually be relatively influent (wet-chemistry synthesis does not easily allow the growth of very long nanowires).

Finally, we found that the output voltage is significantly influenced by the relative dielectric constant surrounding the NW only for very low doping concentrations inside the NW. Our results can be easily generalized for other piezoelectric materials.

Acknowledgments

This research has been supported by the Italian Institute of Technology (Project Seed- API NANE), the Ministero degli Affari Esteri (Direzione Generale per la Promozione e la Cooperazione Culturale), MIUR (MIUR-Interlink project 'Esplorazione delle possibilità applicative di nanostrutture di ossido di zinco per la realizzazione di nanosensori e nano attuatori wireless biocompatibili') and Polo Solare Organico—Regione Lazio. The authors thank Matthias Auf Der Maur for helpful discussions.

References

[1] Wang Z L 2010 Piezotronic and piezophototronic effects *J. Phys. Chem. Lett.* **1** 1388–93
[2] Pan Z W, Dai Z R and Wang Z L 2001 Nanobelts of semiconducting oxides *Science* **291** 1947–9
[3] Wang X, Song J and Wang Z L 2007 Nanowire and nanobelt arrays of zinc oxide from synthesis to properties and to novel devices *J. Mater. Chem.* **17** 711–20
[4] Kong X Y, Ding Y, Yang R and Wang Z L 2004 Single-crystal nanorings formed by epitaxial self-coiling of polar nanobelts *Science* **303** 1348–51
[5] Gao P X, Ding Y, Mai W J, Hughes W L, Lao C S and Wang Z L 2005 Conversion of zinc oxide nanobelts into superlattice-structured nanohelices *Science* **309** 1700–4
[6] Wang Z L and Song J H 2006 Piezoelectric nanogenerators based on zinc oxide nanowire arrays *Science* **312** 242–6
[7] Wang X, Song J and Wang Z L 2007 Direct-current nanogenerator driven by ultrasonic waves *Science* **316** 102–5
[8] Gao P X, Song J, Liu J and Wang Z L 2007 Nanowire piezoelectric nanogenerators on plastic substrates as flexible power sources for nanodevices *Adv. Mater.* **19** 67–72
[9] Yang R, Qin L, Dai L and Wang Z L 2009 Power generation with laterally packaged piezoelectric fine wires *Nature Nanotechnol.* **4** 34–9
[10] Guang Z L, Yang R, Wang A C and Wang Z L 2010 Muscle-driven *in vivo* nanogenerator *Adv. Mater.* **22** 2534–7
[11] Xu S, Qin Y, Xu C, Wei Y, Yang R and Wang Z L 2010 Self-powered nanowire devices *Nature Nanotechnol.* **5** 367–73
[12] Hofmann D M, Hofstaetter A, Leiter F, Zhou H J, Henecker F, Meyer B K, Orlinskii S B, Schmidt J and Baranov P G 2002 Hydrogen: a relevant shallow donor in zinc oxide *Phys. Rev. Lett.* **88** 45504–7
[13] Look D C, Farlow G C, Reunchan P, Limpijumnong S, Zhang S B and Nordlund K 2005 Evidence for native-defect donors in n-type ZnO *Phys. Rev. Lett.* **95** 225502
[14] Van de Walle C G 2000 Hydrogen as a cause of doping in zinc oxide *Phys. Rev. Lett.* **85** 1012–5
[15] Mantini G, Gao Y, D'Amico A, Falconi C and Wang Z L 2009 Equilibrium piezoelectric potential distribution in a deformed ZnO NW *Nano Res.* **2** 624–9
[16] Gao Y and Wang Z L 2009 Equilibrium potential of free charge carriers in a bent piezoelectric semiconductive NW *Nano Lett.* **9** 1103–10
[17] Gao Y and Wang Z L 2007 Electrostatic potential in a bent piezoelectric nw. The fundamental theory of nanogenerator and nanopiezotronics *Nano Lett.* **7** 2499–505
[18] Sun C, Shi J and Wang X 2010 Fundamental study of mechanical energy harvesting using piezoelectric nanostructures *J. Appl. Phys.* **108** 034309
[19] Kobiakov I B 1980 Elastic, piezoelectric and dielectric properties of ZnO and CdS single crystals in a wide range of temperatures *Solid State Commun.* **35** 305–10
[20] Carlotti G, Socino G, Petri A and Verona E 1987 Acoustic investigation of the elastic properties of ZnO films *Appl. Phys. Lett.* **51** 1889–91
[21] Ashkenov N *et al* 2003 *J. Appl. Phys.* **93** 126–33
[22] Falconi C, Mantini G, D'Amico A and Wang Z L 2009 Studying piezoelectric NWs and nanowalls for energy harvesting *Sensors Actuators* B **139** 511–9
[23] www.tibercad.org
[24] Auf Der Maur M, Penazzi G, Romano G, Sacconi F, Pecchia A and Di Carlo A 2011 The multiscale paradigm of multiscale device simulations *IEEE Trans. Electron Devices* **58** 1425–32
[25] Klingshirn C 2007 ZnO: material, physics and applications *ChemPhysChem* **8** 782–803
[26] Yuan D, Guo R, Wei Y, Wu W, Ding Y, Wang Z L and Das S 2010 Heteroepitaxial patterned growth of vertically aligned and periodically distributed ZnO NWs on GaN using laser interference ablation *Adv. Funct. Mater.* **20** 3484–9